Hindawi
Modelling and Simulation in Engineering
Volume 2019, Article ID 2089304, 13 pages
https://doi.org/10.1155/2019/2089304

Research Article

Simulation of the Working Performance of a Shearer Cutting Coal Rock

Li-juan Zhao and Hong-mei Liu

College of Mechanical Engineering, Liaoning Technical University, Fuxin 123000, China

Correspondence should be addressed to Hong-mei Liu; 56104170@qq.com

Received 7 December 2018; Revised 4 February 2019; Accepted 13 February 2019; Published 27 March 2019

Academic Editor: Zhiping Qiu

Taking the MG2∗55/250-BWD shearer as the research object and considering the influence of the rock on the working performance of the shearer, the shearer-coal-rock coupled discrete element model was established and its dynamic working process has been studied. The single-factor analysis method was used to study the variation law of the cutting depth, traction speed, and the drum's rotational speed on the three-way force acting on the drum, the coal loading rate, and the trajectory of the coal particles. The simulation showed that the coal loading rate fluctuated during the start-up phase of the shearer, and it was then constant as the time increased. The value of the cutting resistance was the largest, the traction resistance was the second largest, the axial force was the smallest, and the fluctuation coefficient of the axial force was the largest of all of them. The research showed that the coal loading rate of the drum decreased with the increase of the cutting depth, increased with the increase of the rotating speed of the drum, and decreased with the increase of the traction speed. The three-way force of the drum increased with the increase of the traction speed, decreased with the increase of the drum's rotational speed, and increased with the increase of the cutting depth. According to the analysis of the coal cutting force and the coal loading rate, the drum could achieve high-efficiency cutting if the cutting depth, rotational speed, and traction speed of the dynamic were matched.

1. Introduction

The working mechanism of a shearer has two functions: coal cutting and coal loading. Most of the research on the coal cutting rules of the spiral cutters of coal mining machines has been based on theoretical formulas or experience. However, for shearers that cut coal rock, the loads have strong nonlinear and time-varying properties. The theoretical parameters of the formula have large fluctuations, and the calculation of the load suffers from inevitable human error [1]. LS-DYNA was used in the literature to simulate the drum cutting coal, and the unit was automatically removed after failure [2]; it is difficult to reflect the influence of the reaction on the drum during coal loading, and the discrete element method has certain advantages [3]. The discrete element method was used in the literature to simulate the cutting head [4], and the cutting force variation law of the pick was obtained. The discrete element method was used in the literature to simulate the performance of the cutting head [5], and the cutting force variation law of the pick was obtained, and the reliability of the simulation was verified experimentally. The influence of the roof pressure on the cutting performance was considered in the literature [6], and the discrete element method was used to study the dynamic process of the drum cutting coal rock, and the coal loading rate and force were obtained under different drum motion parameters. The PCF was used in the literature [7] to simulate the uniform linear cutting process of the pick, and the theoretical results of the simulation result are consistent. The discrete element method was used in the literature [8] to study the performance of coal drum loading, and the effects of the spiral drum structure and kinematic parameters on the motion law of the coal loading were obtained. The three-dimensional discrete element software was used in the literature [9] to simulate the vertical screw conveyor, and the effects of speed, blade clearance, and material parameters on

the conveying effect are obtained. The discrete element method was used in the literature [10] to analyze the coal loading performance of the shearer, and the influence of the drum motion parameters on the drum coal loading rate was obtained. The discrete element analysis software PFC3D was used in the literature [11] to simulate the process of the pick breaking the coal, and the force of the pick and the relationship between the force of the pick and the cutting thickness were obtained. The discrete element software was used in the literature [12] to simulate the process of the drum breaking the coal, and the variation law of the coal wall and the force of the drum were obtained during the working process of the double drum shearer. The discrete element software was used in the literature [13] to simulate the charging process of the drum and analyze the factors affecting the drum loading. EDEM was used in literature [14] to simulate the rock fracture problem and obtain the rock failure mechanism. The discrete element software was used in the literature [15] to study the dynamic process of the coal rock being cut by the coal mining machine, and the influence of different cutting angles on the coal loading rate, cutting resistance, and the cutting energy consumption of shearer was studied. EDEM software was used in the literature [16] to establish a discrete element simulation model of the shearer's cutting section, and the relationship between the drum speed, the traction speed, and the coal loading rate was analyzed. The discrete element method was used in the literature [17] to study the dynamic process of picks cutting coal, and the effect of the different cutting thickness on the cutting force was obtained.

2. Discrete Element Theory Analysis

According to the theory of discrete elements [18, 19], the coal wall model uses the Hertz-Mindlin bonding contact model. The bonding of particles 1 and 2 is achieved by the bond as shown in Figure 1; a certain bonding force must be existent between the coal particles by the bond.

In Figure 1, r_1 and r_2 are the radii of particles 1 and 2, respectively, r_{n1} and r_{n2} are the contact radii of particles 1 and 2, U_n is the normal overlap between particles, C_n and C_t are the normal and tangential damping, and S_n and S_t are the normal contact stiffness and tangential contact stiffness between particles, respectively.

$$S_n = 2E^* \sqrt{r^* U_n}, \tag{1}$$

$$S_t = 8G^* \sqrt{r^* U_n}, \tag{2}$$

$$C_n = 2\ln e \sqrt{\frac{S_n m^*}{\pi^2 + \ln^2 e}}, \tag{3}$$

$$C_t = 2\ln e \sqrt{\frac{S_t m^*}{\pi^2 + \ln^2 e}}, \tag{4}$$

where E^* is the equivalent elastic modulus, $1/E^* = (1-\mu_1^2)/E_1 + (1-\mu_2^2)/E_2$, E_1 and E_2 are the macroscopic elastic moduli of particles 1 and 2, respectively, μ_1 and μ_2 are the macroscopic Poisson ratios of particles 1 and 2, G^* is the equivalent elastic modulus, $1/G^* = (2-\mu_1^2)/G_1 + (2-\mu_2^2)/G_2$, and G_1 and G_2 are the macroscopic shear moduli of particles 1 and 2. r^* is the equivalent radius of particles, $1/r^* = 1/r_1 + 1/r_2$. m^* is the equivalent mass of particles, $1/m^* = 1/m_1 + 1/m_2$. e is the restitution coefficient of particles in Table 1.

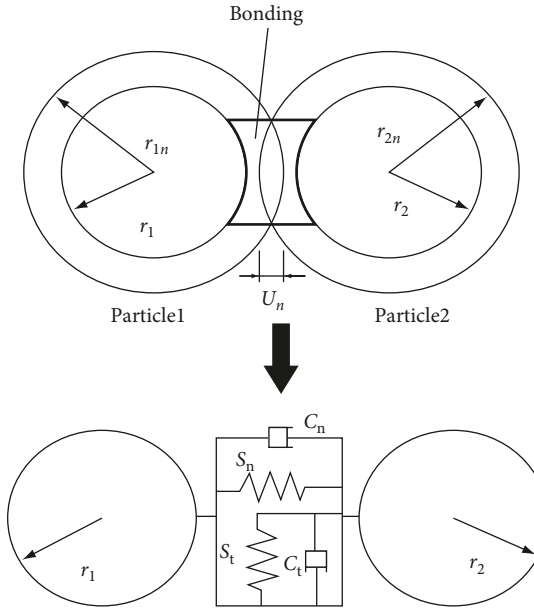

Figure 1: Bonding contact model.

The mathematical expressions of the bonding force and the torque between the particles are shown in the following formula:

$$\begin{cases} \delta F_n = -v_n S_n \delta t, \\ \delta F_t = -v_t S_t \delta t, \\ \delta T_n = -\omega_n S_n J \delta t, \\ \delta T_t = -\omega_t S_t \dfrac{J}{2} \delta t, \end{cases} \tag{5}$$

where δ_t is the time step, v_n is the normal velocity of the particles, v_t is the tangential velocity of the particles, ω_n is the normal angular velocity of the particles, ω_t is the tangent angular velocity of the particles, S_n is the normal contact stiffness of the particles, and S_t is the tangential contact stiffness. Due to the bonding force, the particles can withstand certain stretching and shearing effects. When the force between the particles exceeds the bonding strength, the bond is broken [18], and the breaking conditions are shown in the following formula:

$$\begin{cases} \sigma_{\max} < \dfrac{-F_n}{A} + \dfrac{2T_n}{J} R, \\ \tau_{\max} < \dfrac{-F_t}{A} + \dfrac{2T_t}{J} R, \end{cases} \tag{6}$$

Table 1: Particle parameters of coal rock.

	Dynamic friction coefficient	Static friction coefficient	Recovery coefficient
Coal and coal	0.05	0.8	0.5
Rock and rock	0.05	0.7	0.5
Coal and rock	0.05	0.75	0.5
Coal and drum	0.01	0.5	0.5
Rock and drum	0.01	0.6	0.5

Table 2: Physical and mechanical parameters of coal.

	Density (kg/m^3)	Tensile strength (MPa)	Compressive strength (MPa)	Elastic modulus (MPa)	Poisson's ratio (MPa)	Cohesion	Internal friction angle (°)
Coal	1466.92	2.38	15.43	3940	0.33	4.5	38
Rock	2455.80	6.22	34.62	20960	0.16	14.2	34

where $A = \pi R^2$, $J = (1/2)\pi R^4$, and $R = \sqrt{r_1 r_2}$. R is the bonding radius, F_n and F_t are the normal and tangential forces between the particles, T_n and T_t are the normal and tangential moments between the particles, A is the contact area, and J is the polar moment of inertia.

3. Simulation Model of the Drum Cutting Coal Rock

3.1. Establishment of the Discrete Element Method of the Coal Rock Model. In order to accurately establish the coal wall model, the coal seam samples and rock samples were tested [20], including density, tensile strength, compressive strength, elastic modulus, Poisson's ratio, cohesion, and internal friction angle. The test results of the physical and mechanical parameters of the coal rock are shown in Table 2.

Both the coal and rock used the Hertz-Mindlin bonding contact models. The normal contact stiffness S_n and the tangential contact stiffness S_t were calculated by using equations (1) and (2) and the relevant parameters from Tables 1 and 2. The normal stress σ and tangential stress τ can be calculated by Mohr–Coulomb theory. When the stress value exceeds σ or τ, the corresponding tensile or shear failure or shear failure occurs [21], as shown in the following formula:

$$\begin{cases} \sigma = \dfrac{1}{2}(\sigma_1 + \sigma_3) + \dfrac{1}{2}(\sigma_1 - \sigma_3)\cos 2\alpha, \\ \tau = C + \sigma \tan \varphi, \\ \alpha = \dfrac{\pi}{4} + \dfrac{\varphi}{2}, \end{cases} \tag{7}$$

where σ is the normal stress on the failure surface (MPa), τ is the shear stress of the failure surface (MPa), σ_1 is the maximum principal stress (MPa), σ_3 is the minimum principal stress (MPa), α is the shear failure angle (°), φ is the internal friction angle (°), and C is the cohesion of coal rock (MPa). Among them, σ_1 and σ_3 can be calculated by McClintock and Walsh's modified Griffith formula, as shown in the following formula:

$$\begin{cases} \sigma_1 = -\dfrac{4\sigma_t}{\left(1 - (\sigma_3/\sigma_1)\right)\sqrt{1+f^2} - f\left(1 + (\sigma_3/\sigma_1)\right)}, \\ \dfrac{\sigma_3}{\sigma_c} = \dfrac{\sigma_3}{\sigma_c}\dfrac{\sqrt{1+f^2}+f}{\sqrt{1+f^2}-f} + 1, \end{cases} \tag{8}$$

where σ_t is the tensile strength of the material (MPa), σ_c is the compressive strength of the material (MPa), and f is the coefficient of friction. The normal stress σ and tangential stress τ were calculated by using equations (7) and (8) and the relevant parameters from Table 2. The parameters of the particle contact model [20] are shown in Table 3.

The coal particles were nonuniform and spherical, and the radius of the sphere varied from 6 mm to 18 mm [18]. To establish the coal rock model, it was necessary to first establish a coal wall particle factory and fill it with the coal particles. When the coal particles had been introduced, a virtual rock particle factory was built and the rock particles were introduced. Finally, a virtual coal particle factory was built and the coal particles were introduced. This completed the filling process of the coal wall containing a layer of rock. The filled coal rock model was compressed, so that the distance between the particles reached the contact radius, and the particles were bonded according to the parameters of Table 3, and a three-dimensional model of the bond contact with the rock wall was obtained.

3.2. Establishment of the Drum Model. Taking the spiral drum of the MG2∗55/250-BWD type coal mining machine as the prototype, the three-dimensional solid model of the drum was established in Pro/E, as shown in Figure 2(a), and the picking arrangement diagram of the drum was established as shown in Figure 2(b). The drum model was imported into the discrete element model in the IGES file format.

3.3. Simulation Setup and Solution. According to the actual working conditions, the rotational speed of the drum was 95 r/min, and the traction speed was 4 m/min. In order to ensure the stability of the simulation, the time step should be

Table 3: Particle contact model parameters.

	Normal stiffness (N/m)	Tangential stiffness (N/m)	Normal stress (MPa)	Tangential stress (MPa)
Coal and coal	1.13×10^8	9.01×10^7	8.32	2.36
Rock and rock	1.98×10^8	1.59×10^8	26.4	13.30
Coal and rock	1.44×10^8	1.15×10^8	17.00	7.40

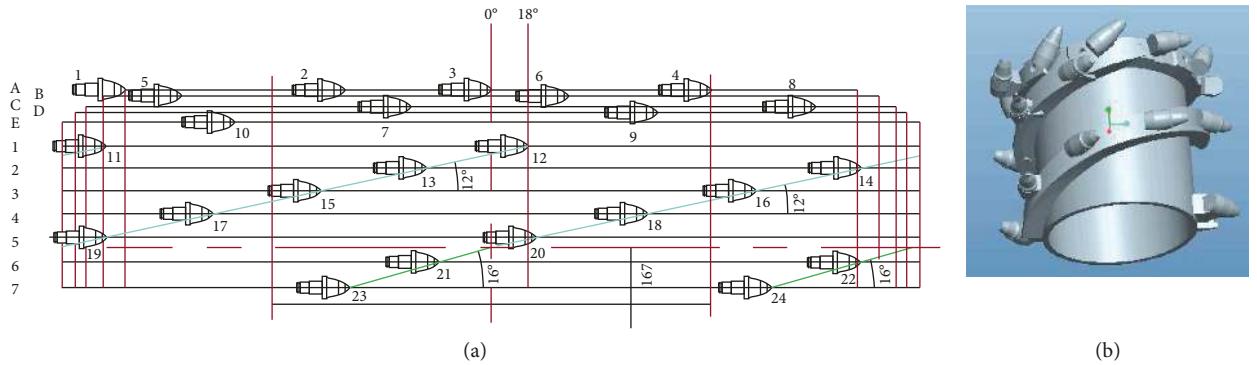

(a) (b)

Figure 2: (a) The picking arrangement diagram of the drum (b) Three-dimensional model of the drum.

appropriate, and the Rayleigh time step [22] is the maximum of the time step of particle set, determined by

$$T_R = \pi r\left(\frac{\rho}{G}\right)^{1/2}(0.1631\mu + 0.8766)^{-1}, \quad (9)$$

where T_R is the Rayleigh time step, r is the coal particle radius, ρ is the particle density, G is the shear modulus, and μ is the Poisson ratio. The time step is usually set from the range of 10 to 40%T_R. In this paper, the time step was 20%T_R. Rayleigh time step was calculated as $3.42e-06$ s. The simulation time was 6 s, the target storage time interval was 0.01 s, and the grid size was 5 times that of the minimum particle radius, and the coal mining machine cutting coal rock process is shown in Figure 3.

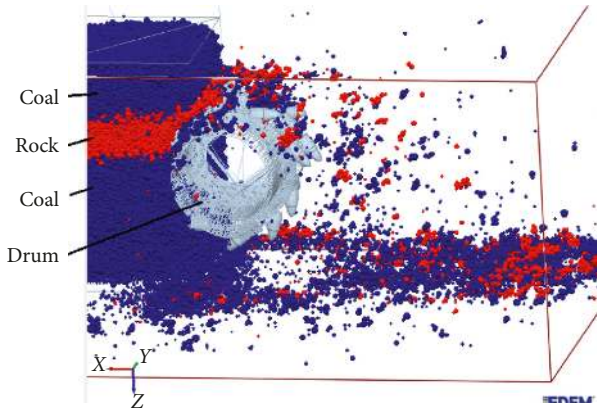

Figure 3: The model of the drum cutting coal containing a dirt band.

4. Analysis of the Simulation Results

4.1. Analysis of the Three-Dimensional Force of the Drum. In the EDEM postprocessing, the three-directional force and the total force of the drum were extracted and exported as a .CVS file, and the three-dimensional force curve was obtained in MATLAB, as shown in Figure 4. It can be seen from Figure 4(a) that when the drum cut the coal rock, the total force fluctuated irregularly within a certain range. This was because the position, number, and declination of the picks involved in the cutting were constantly changing with time, and the coal rock was not regular. In the three-directional force, the Z-direction force was the cutting resistance, the X-direction force was the traction resistance, and the Y-direction force was the axial force. Among them, the value of the cutting resistance was the largest, the traction resistance was second, and the axial force was the smallest, as shown in Figure 4(b). The Y-direction force of the drum fluctuated above and below zero, but its average value was not zero.

4.2. Force Analysis of Each Intercept Pick. It can be seen from the pick arrangement diagram of the drum that the barrel had 7 sections and the end plate had 5 sections. In the postprocessing of EDEM, the force of each pick was extracted and collated by MATLAB Figure 5.

4.3. The Influence of the Rotational Speed, the Traction Speed, and the Cutting Depth on the Triaxial Force of the Drum

4.3.1. Influence of the Rotational Speed on the Triaxial Force of the Drum. In order to obtain the relationship between the rotational speed and the triaxial force, the simulations were carried out with different rotational speeds of 75 r/min, 85 r/min, 95 r/min, and 105 r/min and a traction speed of 4 m/min. The load fluctuation coefficient [23, 24] can measure the cutting performance of the drum. The load fluctuation coefficient is

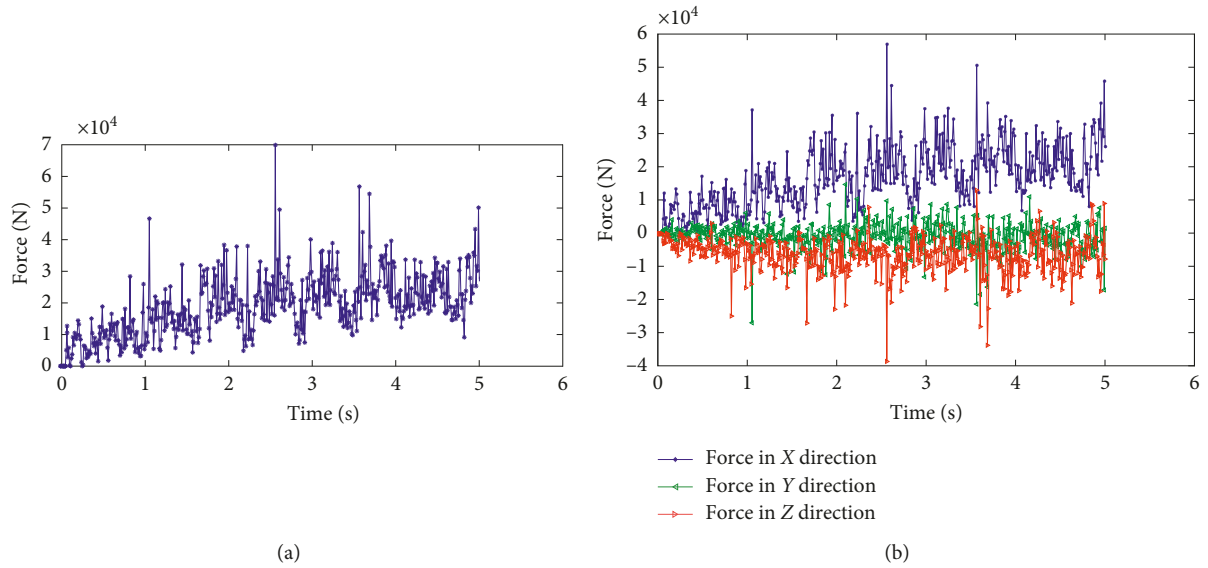

Figure 4: (a) The total force of the drum. (b) Three-directional force of the drum.

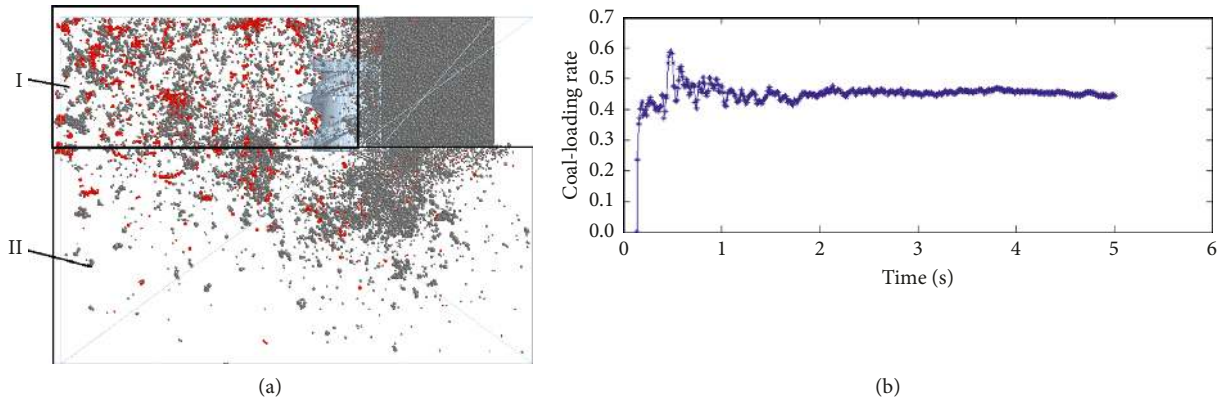

Figure 5: The total force of the teeth. The force of the (a) 11th and 12th teeth; (b) 13th and 14th teeth; (c) 15th and 16th teeth; (d) 17th and 18th teeth; (e) 19th and 20th teeth; (f) 21st and 22nd teeth; (g) 23rd and 24th teeth; (h) 10th tooth; (i) 9th tooth; (j) 7th and 8th teeth; (k) 5th and 6th teeth; (l) 1st, 2nd, 3rd, and 4th teeth.

$$\delta = \frac{1}{\overline{F}}\sqrt{\frac{1}{r}\sum_{i=1}^{r}\left(F_i - \overline{F}\right)^2}, \qquad \overline{F} = \frac{1}{r}\sum_{i=1}^{r}F_i, \tag{10}$$

where F_i is the instantaneous value of the drum load and $\overline{F}$ is the average of the drum load. The three-way extraction force is shown in Table 4. It can be seen from Table 4 that the average value of the three-way resultant force decreased with the increase of the rotational speed; when the traction speed and the depth of the cut were constant, the rotational speed of the drum increased, the cutting thickness decreased, and the corresponding cutting resistance decreased.

4.3.2. Influence of the Traction Speed on the Three-Way Force of the Drum. In order to obtain the relationship between the traction speed and the triaxial force, the simulations were carried out with different traction speeds of 3 m/min, 4 m/min, 5 m/min, and 6 m/min, and the speed of the drum was 95 r/min. The three directions of the drum were extracted in postprocessing. The force and the three-way force were collated by MATLAB, as shown in Table 5. It can be seen from Table 5 that the average value of the resultant three-way force increased with the increase of the traction speed. Due to the increase of the traction speed, when the rotational speed was constant, the maximum cutting thickness of the drum increased, and the force received by the drum cutter per unit time also increased, so the resultant force increased.

4.3.3. Influence of the Cutting Depth on the Three-Way Force of the Drum. In order to obtain the relationship between the cutting depth and the triaxial force, simulations were carried out with different cutting depths of 480 mm, 530 mm,

Table 4: The relationship between the rotational speed and the three-directional force of the drum.

Rotational speed (r/min)	X-force (mean/N)	Fluctuation coefficient of X-force	Y-force (mean/N)	Fluctuation coefficient of Y-force	Z-force (mean/N)	Fluctuation coefficient of Z-force	Resultant force (mean/N)	Fluctuation coefficient
75	−6.52e3	−0.0104	1.08e2	0.3406	1.17e4	0.0076	2.0154e4	0.0364
85	−6.12e3	−0.0111	−3.03e2	−0.1650	1.12e4	0.0077	1.9351e4	0.0275
95	8.28e3	−0.0093	−5.98e2	−0.102	1.65e4	0.0062	1.9180e4	0.0373
105	−5.82e3	−0.0116	−1.52e2	−0.3480	1.06e4	0.0085	1.8547e4	0.0341

Table 5: The relationship between the traction speed and the three-directional force of the drum.

Traction speed/ m/min	X-force (mean/N)	Fluctuation coefficient of X-force	Y-force (mean/N)	Fluctuation coefficient of Y-force	Z-force (mean/N)	Fluctuation coefficient of Z-force	Resultant force (mean/N)	Fluctuation coefficient
3	−6.14e3	−0.0106	−1.72e2	−0.3065	1.11e4	0.0078	1.3181e4	0.0348
4	−8.28e3	−0.0093	−5.98e2	−0.1020	1.65e4	0.0062	1.9180e4	0.0373
5	−9.18e3	−0.0085	−7.54e2	−0.0862	2.20e4	0.0053	2.4518e4	0.0363
6	−1.29e4	−0.0064	−5.58e2	−0.1124	2.91e4	0.0043	3.2393e4	0.0368

Table 6: The relationship between the cutting depth and the three-directional force of the drum.

Cutting depth/ mm	X-force (mean/N)	Fluctuation coefficient of X-force	Y-force (mean/N)	Fluctuation coefficient of Y-force	Z-force (mean/N)	Fluctuation coefficient of Z-force	Resultant force (mean/N)	Fluctuation coefficient
480	−6.84e3	−0.0355	−9.28e2	−0.293	1.25e4	0.0311	1.4733e4	0.0312
530	−6.59e3	−0.0361	−8.24e2	−0.282	1.36e4	0.0314	1.5902e4	0.0305
580	−7.08e3	−0.0347	−6.35e2	−0.258	1.48e4	0.0306	1.6973e4	0.0293
630	−8.28e3	−0.0093	−5.98e2	−0.102	1.65e4	0.0062	1.9180e4	0.0373

580 mm, and 630 mm, and the traction speed was 4 m/min, and the drum's speed was 95r/min. The three-way resultant force of the extraction drum was extracted and sorted by MATLAB. The results are shown in Table 6. It can be seen from Table 6 that the average value of the three-way force of the drum increased with the increase of the cutting depth. When the cutting depth of the cut increased, the number of picks involved in the cut increased, causing the resultant force of the drum to increase.

4.4. Research on the Performance of Drum Loading. Statistics on the particle mass of the floating coal zone I and the effective coal loading area II have been shown in Figure 6(a). The total amount of coal falling was the sum of the particle mass in the effective coal loading zone and the floating coal zone [25]. The coal loading rate η is the mass of the effective coal loading area divided by the total mass of falling coal, as shown in the following equation:

$$\eta = \frac{m_e}{m_e + m_f}, \tag{11}$$

where m_e is the particle mass of the loading coal zone and m_f is the particle mass of the floating coal zone. When the drum's rotational speed was 95 r/min, the traction speed was 4 m/min and the cutting depth was 580 mm; the drum's coal loading rate curve is shown in Figure 6(b). It can be seen from Figure 6(b) that the coal loading rate fluctuated a certain amount during the start-up phase of the shearer, and the coal loading rate became constant as the time increased.

4.4.1. Influence of Rotational Speed on the Drum Loading Rate. In order to study the effect of the rotational speed on the drum loading rate, the rotational speeds used were 75 r/min, 85 r/min, 95 r/min, and 105 r/min, the cutting depth was 630 mm, the traction speed was 4 m/min, and the simulation was then carried out. In the EDEM posttreatment, the coal flow velocity of 4.45 s in the four working conditions was obtained [26] as shown in Figure 7. It can be seen from Figure 7 that the rotational speed increased from 75 r/min to 105 r/min, and the instantaneous maximum velocity of the coal particles increased from 9.81 m/s to 15.6 m/s, mainly because the cut coal rock was driven by the drum. When the rotational speed of the drum was large, the particles were thrown outward under the frictional force of the drum, and the maximum throwing speed of the particles increased.

In order to analyze the instantaneous velocity and the throwing position of the particles, the distance vs. velocity diagram of the particles obtained for each working condition in the postprocessing is shown in Figure 8. As can be seen from Figure 5, the maximum number of particles of the instantaneous velocity of the coal flow in Figure 8 was small. At most, the instantaneous velocity of the particles

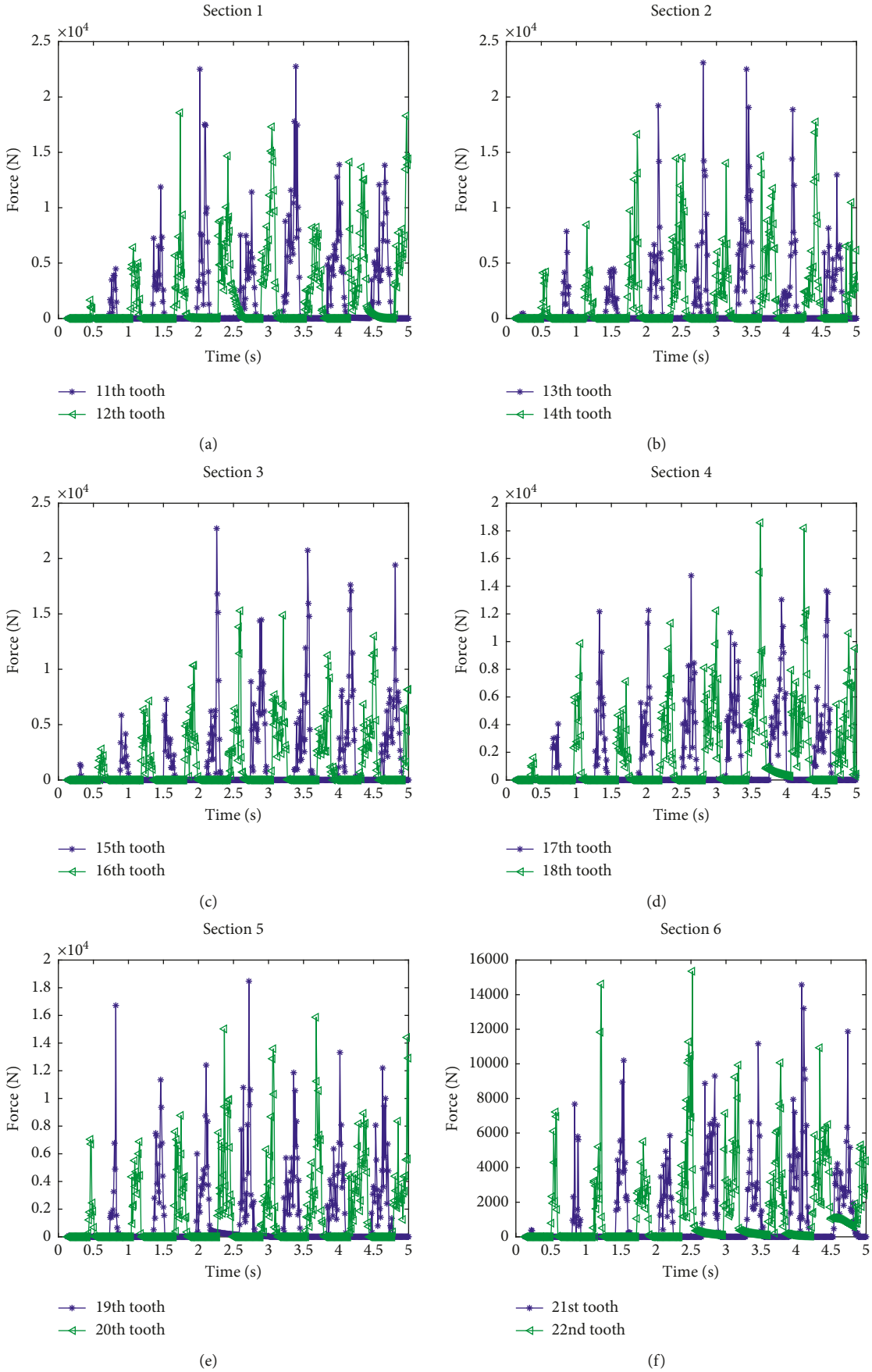

Figure 6: Continued.

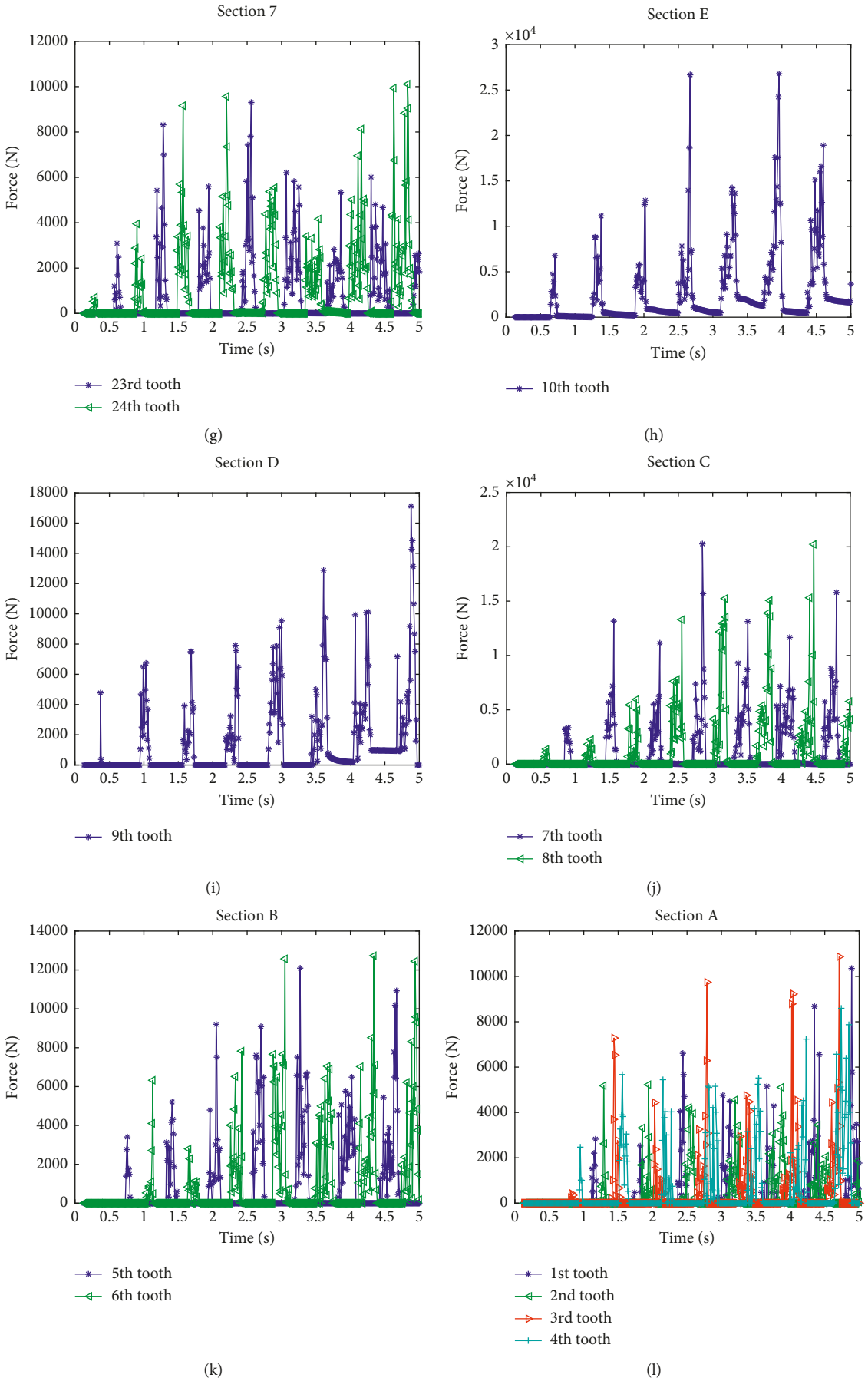

Figure 6: (a) Statistics zone. (b) The coal loading rate curve.

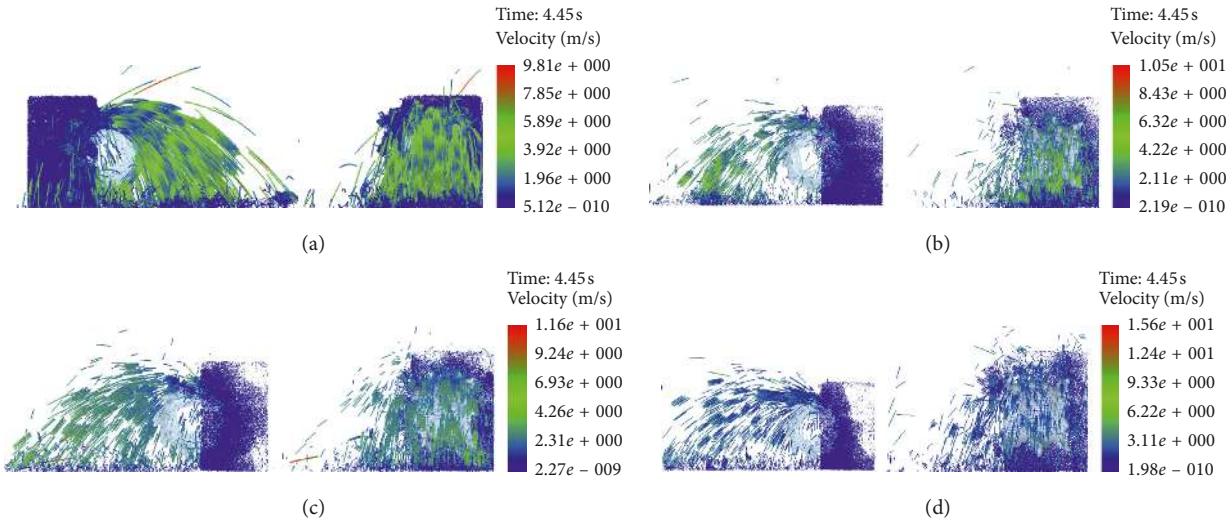

Figure 7: Velocity of the coal particles. (a) $n = 75$ r/min. (b) $n = 85$ r/min. (c) $n = 95$ r/min. (d) $n = 105$ r/min.

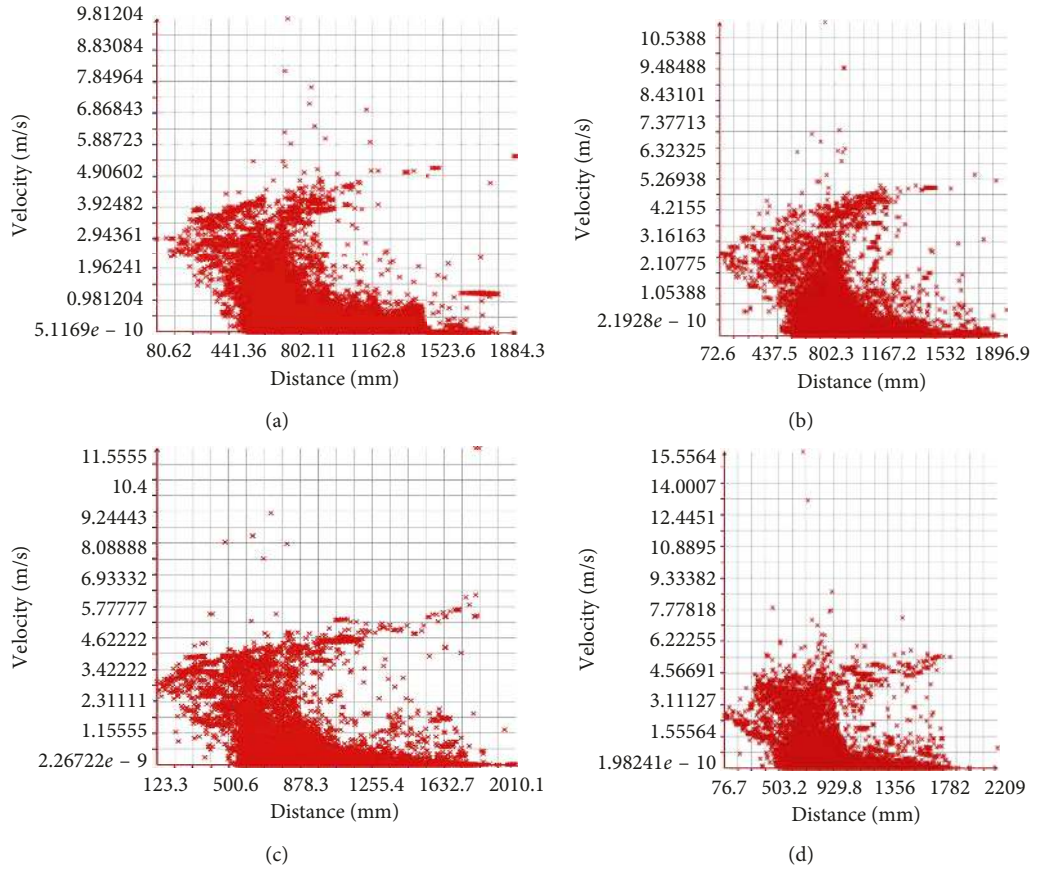

Figure 8: Distance vs. velocity of the coal particles. (a) $n = 75$ r/min. (b) $n = 85$ r/min. (c) $n = 95$ r/min. (d) $n = 105$ r/min.

did not exceed 7 m/s at the same time. The drum had a depth of 630 mm and the coal wall had a width of 800 mm. It can be seen from Figure 5 that the number of effective coal loading zones was different when the cylinder speed was different.

The coal loading rate statistics are shown in Table 7. As can be seen from Table 7, as the drum's rotational speed increased, the coal loading rate gradually increased. Since the speed of the drum was low, the movement of the particles in the drum was mainly sliding, and the speed of particle ejection was small. As the rotational speed of the drum increased, the movement of the particles was more affected by the rotation of the drum, so that the particles were thrown into the effective coal loading area, so the coal loading rate improved.

Table 7: The statistics of the coal loading rate.

Traction speed (m/min)	Rotational speed (m/r/min)	Cutting depth (mm)	Average coal loading rate (%)
4	75	630	41.68
	85		43.23
	95		45.59
	105		48.77
3	95		46.68
4			45.59
5			44.21
6			43.45
4		480	56.90
		530	50.061
		580	49.33
		630	45.59

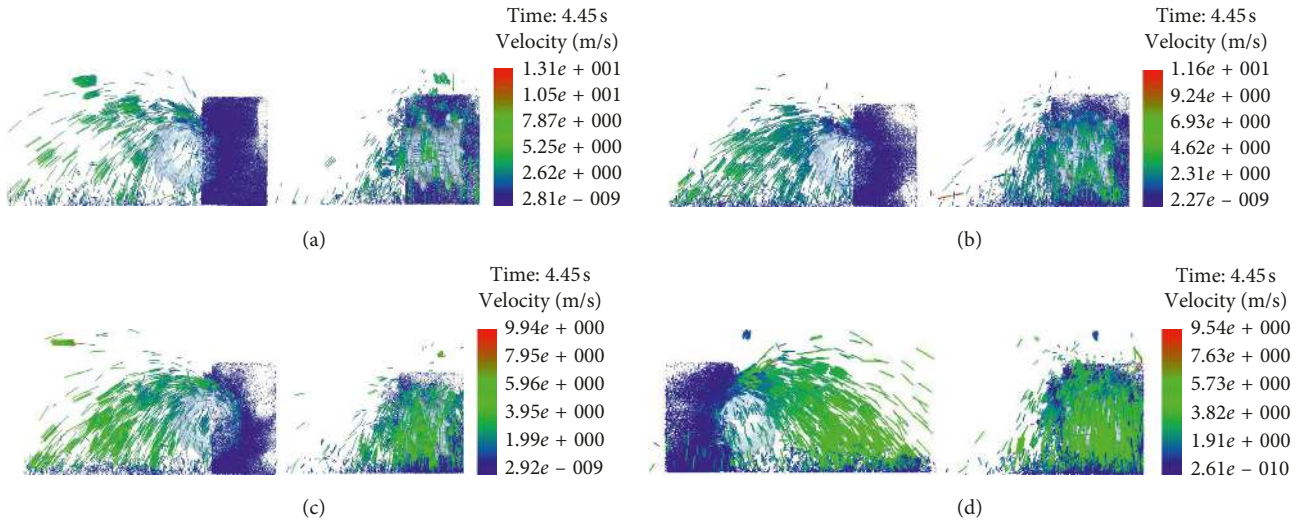

Figure 9: Velocity of the coal particles. (a) $V_q = 3$ m/min. (b) $V_q = 4$ m/min. (c) $V_q = 5$ m/min. (d) $V_q = 6$ m/min.

4.4.2. Influence of Traction Speed on the Drum Loading Rate. In order to study the influence of the traction speed of the drum on the coal loading rate of the drum, the drum speed was set to 95 r/min, the cutting depth was 630 mm, the traction speeds used were 3 m/min, 4 m/min, 5 m/min, and 6 m/min, and the simulation was then carried out. The coal particle velocity of the drum obtained in the posttreatment is shown in Figure 9. It can be seen from Figure 9 that as the traction speed increased, the number of coal rock particles falling into the effective coal loading zone gradually increased. However, the traction speed was too large so the amount of coal falling into the floating coal zone increased, so the coal charging rate was lowered. The distance vs. speed of the coal flow is shown in Figure 10. As can be seen from Figure 10, as the traction speed increased, the velocity of most of the particles in each working condition gradually increased. Mainly due to the higher traction speed, the thickness of the drum cutting layer per unit time increased, and the corresponding instantaneous throwing particle speed increased.

The coal loading rate of the abovementioned working condition for the drum is shown in Table 7. It can be seen from Table 7 that as the traction speed of the drum increased, the loading rate of the drum decreased. As the traction speed increased, the coal flow rate in the drum blades increased, which reduced the amount of coal rock that could not be discharged by the coal wall and the picks due to the low traction speed. As the traction speed continued to increase, the unit interception coal volume of the shearer exceeded the coal retention space in the drum blade, causing the coal rock flow to block the drum, and it could not be discharged in time, which greatly reduced the coal loading rate of the drum.

4.4.3. Influence of the Cutting Depth on the Drum Loading Rate. In order to study the effect of the cutting depth on the speed of the coal particles, the rotational speed of the drum was set to 95r/min, the traction speed was set to 4 m/min, and the different depths used were 480 mm, 530 mm, 580 mm, and 630 mm. The coal particle velocity and coal particle distance were obtained for the different depths. The speeds are shown in Figures 11 and 12. It can be seen from Figures 11 and 12 that as the depth of cut increased, the amount of coal particles thrown into the coal charging zone gradually decreased. It can be seen from Table 5 that as the

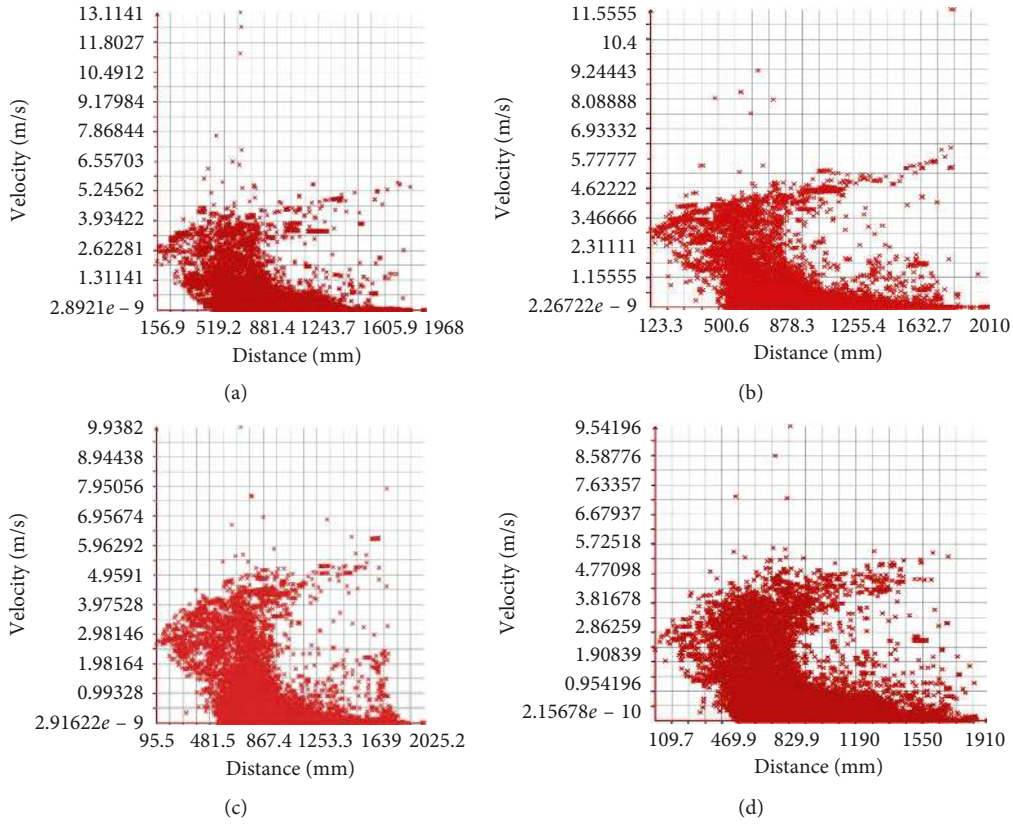

Figure 10: Distance vs. velocity of the coal particles. (a) $V_q = 3$ m/min. (b) $V_q = 4$ m/min. (c) $V_q = 5$ m/min. (d) $V_q = 6$ m/min.

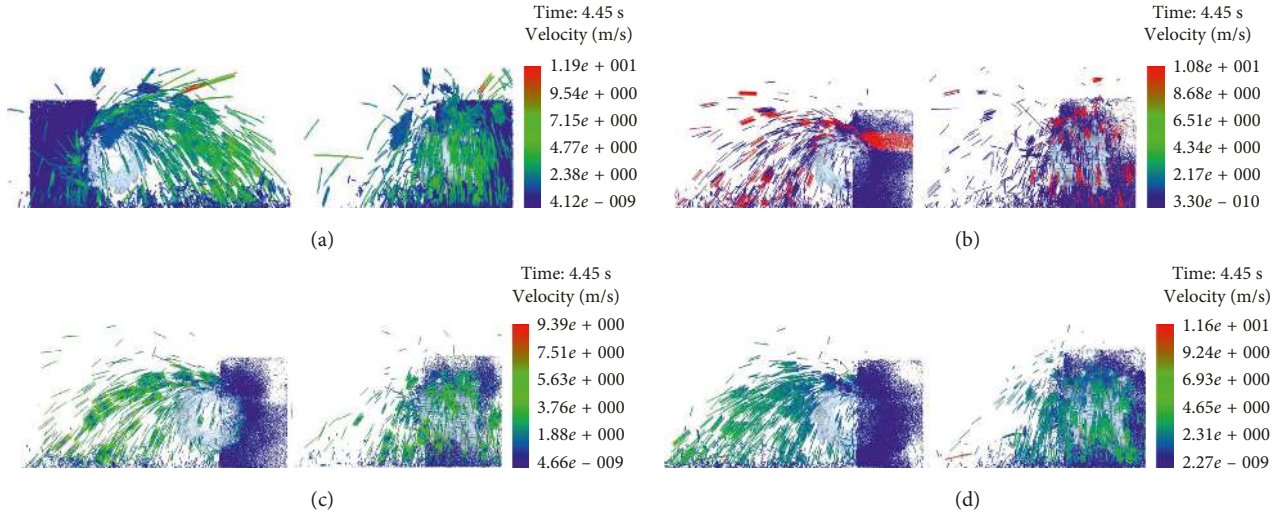

Figure 11: Velocity of the coal flow. (a) $B = 480$ mm. (b) $B = 530$ mm. (c) $B = 580$ mm. (d) $B = 630$ mm.

cutting depth of the shearer deepened, the coal loading rate of the drum was reduced. The main reason for this was that the mining depth of the shearer drum was too large, resulting in a cumulative increase of the amount of coal falling in the capacity space of the drum blade, causing long-term blockage, which was difficult to clear, and increased the drum's resistance.

5. Conclusion

(1) The discrete element analysis software was used to study the dynamic cutting process of coal mining with a shearing coal drum, and it could dynamically observe the rock fragmentation and coal rock velocity trajectory, and it has provided a new

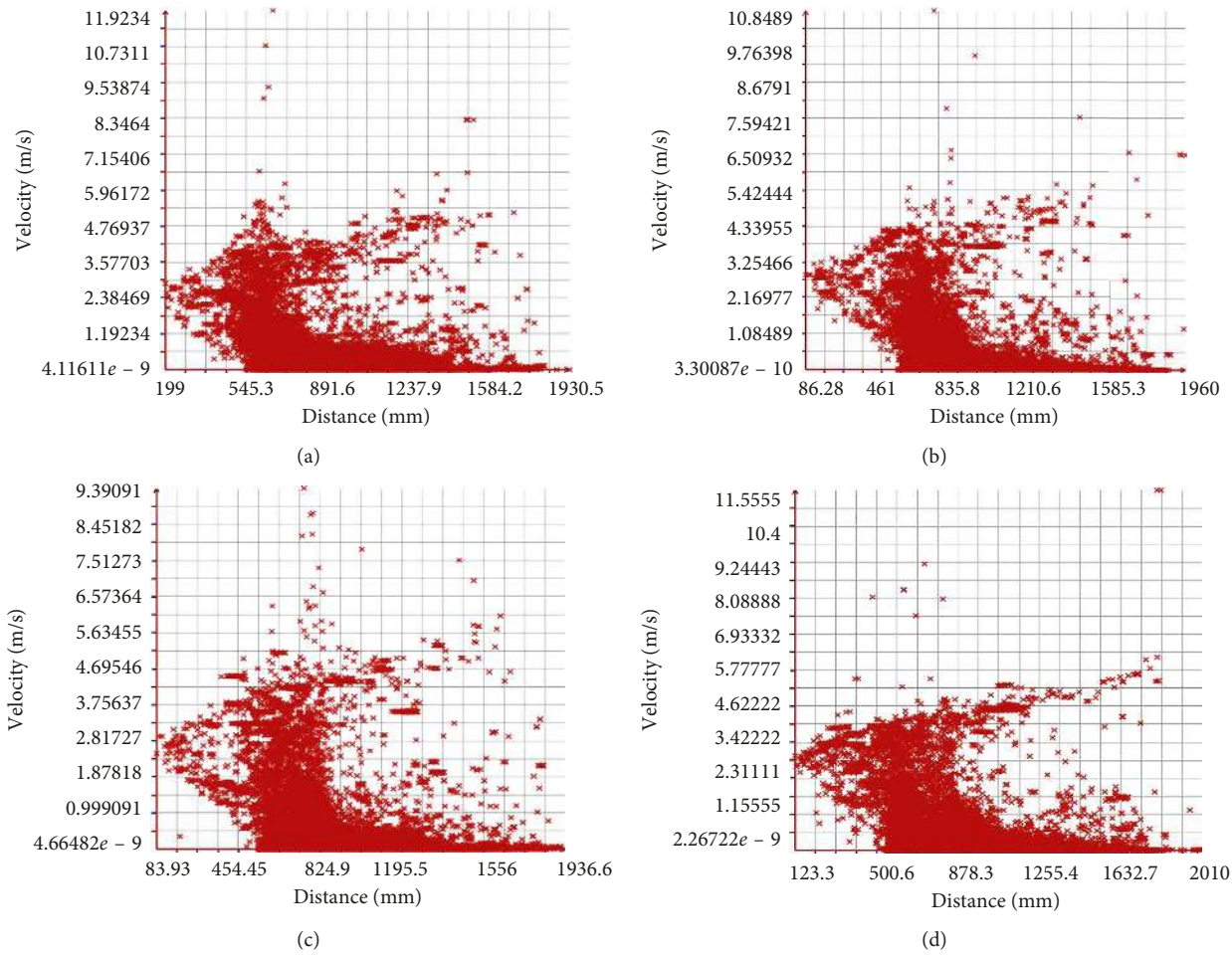

Figure 12: Distance vs. velocity of the coal particles. (a) $B = 480$ mm. (b) $B = 530$ mm. (c) $B = 580$ mm. (d) $B = 630$ mm.

method for studying the working performance of a shearer.

(2) The research indicated that the coal loading rate of the drum decreased with the increase of the depth of cut, increased with the increase of the rotating speed of the drum, and decreased with the increase of the pulling speed. The three-way force of the drum increased with the increase of the traction speed, decreased with the increase of the drum's rotational speed, and increased with the increase of the depth of cut.

(3) It can be seen from the analysis of the coal cutting force and the coal loading rate of the drum cutting that the drum could achieve high-efficiency cutting if the cutting depth, rotational speed, and traction speed were dynamically matched.

Data Availability

The data used to support the findings of this study are available from the corresponding author upon request.

Conflicts of Interest

The authors declare that they have no conflicts of interest.

Acknowledgments

This work was supported by National Natural Science (51674134) and Liaoning Provincial Education Department (LJ2017QL017).

References

[1] L. Zhao and M. Dong, "Load problems of working mechanism of the shearer in containing pyrites and tin coal seam," *Joumal of China Coal Society*, vol. 34, no. 6, pp. 840–844, 2009.

[2] J. He and Z. Wang, "Numerical simulation of coal cutting process of thin coal seam shearer spiral drum," *Coal Engineering*, vol. 6, pp. 97–99, 2013.

[3] R. Li, *DEM Simulation Study of Cutting Coal for the Cutting Header*, Shenyang Ligong University, Shenyang, China, 2014.

[4] Y. Ji and X. Cao, "DEM simulation method study for picks cutting coal of roadheader," *Journal of liaoning engineering technology university (natural science edition)*, vol. 302, no. 4, pp. 488–492, 2013.

[5] K.-D. Gao, *Study on Coal-Loading Performance of Thin Coal Seam Shearer*, China University of Mining and Technology, Xuzhou, China, 2014.

[6] J. Mao, X. Liu, H. Chong et al., "Simulation research of shearer drum cutting performance based on EDEM," *Journal of China Coal Society*, vol. 42, no. 4, pp. 1069–1077, 2017.

[7] O. Su and N. Ali Akcin, "Numerical simulation of rock cutting using the discrete element method," *International Journal of Rock Mechanics and Mining Sciences*, vol. 48, no. 3, 2010.
[8] Z. Tian, L. Zhao, X. Liu et al., "Loading performance of spiral drum based on discrete element method," *Journal of China Coal Society*, vol. 42, no. 10, pp. 2758–2764, 2017.
[9] W. McBride and P. W. Cleary, "An investigation and optimization of the "OLDS" elevator using discrete element modeling," *Powder Technology*, vol. 193, no. 3, pp. 216–234, 2009.
[10] L. Zhao, Z. Tian, W. Bao et al., "A New Method of EDEM on thin seam shearer loading performance and application based on," *Journal of Mechanical Strength*, vol. 39, no. 3, pp. 663–667, 2017.
[11] H. Wu, C. Cheng, C. Ji et al., "Discrete element method analysis of pick cutting coal seam based on PFC3D," *Coal Mine Machinery*, vol. 36, no. 10, pp. 134–136, 2015.
[12] J. Bao, Y. Wang, and Y. Zhang, "Simulation analysis of working process for double drum-type shearer via discrete element method," *Coal Mine Machinery*, vol. 39, no. 7, pp. 60–62, 2018.
[13] C. Wang, "Research of shearer drum loading simulation based on DEM," *Coal Technology*, vol. 37, no. 1, pp. 232–234, 2018.
[14] D. A. Estay and L. E. Chiang, "Discrete crack model for simulating rock comminution processes with the Discrete Element Method," *International Journal of Rock Mechanics and Mining Sciences*, vol. 60, pp. 125–133, 2013.
[15] J. Mao, X. Liu, H. Chen et al., "Different installation angle of cutting picks affected to cutting performances of coal shearer," *Coal Science and Technology*, vol. 45, no. 10, pp. 144–149, 2017.
[16] X. Liu, L. Zhao, F. Renjin et al., "Research on kinematic parameter optimum matching of thin coal seam shearer," *Mechanical Science and Technology for Aerospace Engineering*, vol. 36, no. 11, pp. 1701–1707, 2017.
[17] X. Zhang, Y. Wang, and Z. Yang, "Simulation and analysis on coal cutting process based on EDEM," *Coal Technology*, vol. 34, no. 8, pp. 243-244, 2015.
[18] G. Wang, H. Wanjun, and J. Wang, *Discrete Element Method and its Practice on EDEM*, Northwestern Polytechnical University Press, Xi'an, China, 2010.
[19] J. Liu, C. Ma, Q. Zeng, and K. Gao, "Discrete element simulation of conical pick's coal cutting process under different cutting parameters," *Shock and Vibration*, vol. 2018, Article ID 7975141, 9 pages, 2018.
[20] T. Qu, J. Jiang, and L. Zhao, *The Key Technology of High Efficiency Fully Mechanized Mining in Complex Structure Thin Coal Seam*, China University of Mining and Technology press, Xuzhou, China, 2010.
[21] Q. Lei, *Based on Discrete Element Material Crushing Mechanism Research*, Jiangxi University of Science and Technology, Ganzhou, China, 2012.
[22] J. Quist and C. M. Evertsson, *Cone Crusher Modeling and Simulation*, Department of Product and Production Development, Chalmers University of Technology, Gothenburg, Sweden, 2012.
[23] L. Xia, *Study of Vibration Compression Breakage Process base on Multi-Scale Cohesive Particle Model*, Jiangxi University of Science and Technology, Jiangxi, China, 2016.
[24] L. Zhao, Z. Fan, and W. Zhou, "Study on reliability of spiral drum in the breaking and falling process of coal and rock," *Journal of Safety Science and Technology*, vol. 13, no. 7, pp. 100–105, 2017.
[25] C. Xu, Y. Wang, Z. Yang et al., "Research on the particle movement behavior in coaling process of drum reversion," *Mining Research and Development*, vol. 37, no. 5, pp. 104–108, 2017.
[26] Z. Qu, *Optimization Design Research for Parameter of the Shearer Screw Drum*, Northeastern University, Shenyang, China, 2008.